

EDINBURGH
INSTRUMENTS



PRECISION RAMAN

Best-in-class Raman microscopes
for research and analytical requirements
backed with world-class customer
support and service.



edinst.com

P. Santos Inês P. (Orcid ID: 0000-0003-2463-246X)

Unravelling pine response to *Fusarium circinatum* through Raman spectroscopy

Daniel Martín^{1±}, Inês P. Santos^{1*±}, Pedro Monteiro^{2±}, Joana Amaral^{2±}, Ricardo M.F. da Costa¹, Jorge Martín-García^{3,4}, Luís A.E. Batista de Carvalho¹, Maria Paula M. Marques^{1,5}, Glória Pinto^{2*}

¹ Molecular Physical-Chemistry R&D Unit, University of Coimbra, 3004-535 Coimbra, Portugal

² Centre for Environmental and Marine Studies (CESAM), Department of Biology, University of Aveiro, 3810-193 Aveiro, Portugal

³ Sustainable Forest Management Research Institute, University of Valladolid – INIA, Avenida de Madrid 44, Palencia, Spain

⁴ Department of Plant Production and Forest Resources, University of Valladolid, Avenida de Madrid 44, 34071 Palencia, Spain

⁵ Department of Life Sciences, University of Coimbra, 3000-456 Coimbra, Portugal

±D. Martín, I.P. Santos, P. Monteiro and J. Amaral contributed equally to this work as first authors.

*Corresponding authors (Email: ips@uc.pt; gpinto@ua.pt)

Abstract: Pine Pitch Canker (PPC), caused by the fungus *Fusarium circinatum*, is associated to significant economic and ecological losses worldwide. The effectiveness of PPC monitoring, early detection in nurseries and plantations, and the identification of resistant plant material relies on the development of objective, non-destructive and cost-effective tools. This study analysed the potential of employing Raman Spectroscopy (RS) for the early detection of biochemical changes associated with PPC in *Pinus* spp. with different susceptibilities to *F. circinatum* (highly susceptible *Pinus radiata* vs. relatively-resistant *Pinus pinea*), while unveiling possible mechanisms of action on these pathosystems. Our results indicate lignin as a key constitutive component of pine resistance against PPC and thus the potential of using this technology for the selection of PPC resistant trees. Moreover, we demonstrate the power of RS-based approaches for the rapid detection of the disease in susceptible species. Early spectral variations were found in *P. radiata* upon inoculation with *F. circinatum* from 3 days post-inoculation (dpi) onwards, whereas changes in histological analysis, relative internal stem necrosis measurements, and visual disease symptoms were only visible at 6, 8, and 9-dpi, respectively. These spectral changes have been associated to cell-wall degradation and induction of phenolic compounds synthesis upon infection in *P. radiata*. Altogether, we believe that RS is an innovative promising tool able to reduce disease detection time in pine species and providing an appealing alternative for the development of new and eco-friendly disease control measures.

Keywords: Pine pitch canker; *Pinus* spp., disease detection; species selection; plant protection.

This article has been accepted for publication and undergone full peer review but has not been through the copyediting, typesetting, pagination and proofreading process which may lead to differences between this version and the Version of Record. Please cite this article as doi: 10.1002/jrs.6446

1. Introduction

Forests cover nearly 31% of the total land area worldwide (4.06 billion ha) representing an important economic, environmental, and social asset ^[1]. European forests, in particular, are largely composed of conifers (227 million ha), with pine species representing the greatest growing stock^[2]. These face a growing threat from pests and diseases, especially due to globalization and climate change, which provide potential opportunities for pathogens to colonize new environments ^{[1] [2]}.

Pine Pitch Canker (PPC), caused by the fungal pathogen *Fusarium circinatum* (Nirenberg & O'Donnell), is one of the most important diseases affecting conifers worldwide^[3]. It impacts more than 60 *Pinus* spp. and *Pseudotsuga menziesii* (Mirb.) Franco, at all stages of tree development, causing significant ecological and economic losses^[3-5]. The typical symptomatology of PPC is needle discoloration, tip dieback and excessive resin-soaking ^[3]. Fungal infection occurs mainly through wounds on host tissues. From there, *F. circinatum* colonizes the host radially advancing towards the pith, likely through the release of cell wall degrading enzymes, but also vertically after reaching the phloem or the traumatic resin ducts formed in the xylem^[6]. The increased resin production observed, together with the physical obstruction by *F. circinatum* growth, and the generalized cell death occurring in the xylem after infection, may lead to restricted water supply and eventually result in host death^[7,8]. Although *F. circinatum* is currently subjected to quarantine measures in Europe (List A2; locally present but not widely distributed in the Euro-Mediterranean region), there are still no effective management and control tools against PPC^[9].

In line with the EU 2030 directives for tree protection ^[10], exploiting hosts' genetic resistance to PPC based on intra- and inter-specific variance in order to select and/or develop PPC resistant trees is, together with early detection, one of the most promising and environmental-friendly measures to control the disease ^[9-12]. To achieve this resistance it is crucial to study hosts with varying levels of susceptibility to the disease in order to identify resistance mechanisms and specific signatures, candidate genes or metabolic pathways for further selection and/or manipulation ^[15]. Several transcriptomic studies contributed with new insights that fill this knowledge gap in PPC ^[14-17]. These have recently been complemented with physiological, multi-Omics and rhizobiome studies comparing one of the most PPC susceptible pine species (*Pinus radiata* D. Don) with a relatively resistant one (*Pinus pinea* L.) aiming to explore the onset of disease and identify specific mechanisms that may explain the differential responses observed ^{[12,13,20][21][22]}. However, advances on the development of early detection tools for PPC are still lacking.

The monitorization and early detection of plant diseases, as well as the identification of resistant plant material, are dependent on the availability of rapid, reliable and cost-effective tools prone to be adapted for high-throughput sampling^{[23][24]}. Optical vibrational spectroscopy has been employed to assess both the chemical fingerprint of metabolites (using Fourier-transform mid-infrared (FTIR) spectroscopy) and lignocellulosic components (through Raman spectroscopy, RS)^[25]. FTIR spectroscopy has been successfully applied to distinguish differential disease-responsive plants, *via* specific spectral signatures analysed by dedicated chemometric methods^[26]. Several studies reported the use of FTIR spectroscopy to either discriminate hosts with varying levels of susceptibility to forest tree diseases (such as the Dutch elm disease, Diplodia tip blight, and ash dieback ^[27-31]), or for the early detection of disease in

the Norway spruce-*Heterobasidion annosum* pathosystem [32]. RS, in turn, has recently attracted research interest due to its unique advantages in practical applications within this field, namely low-cost and simplicity regarding sample preparation, allowing *in situ* analysis facilitated by the portability of RS spectrometers [33] [34]. Therefore, RS has been employed for species-specific analysis and differentiation against abiotic stress in agriculture [35], providing specific biochemical fingerprints associated to chemical and structural alterations that may be linked to particular phenotypic markers of disease [35],[36].

In this study, RS coupled to histological analysis have been applied to characterize disease progression in seedlings of both the PPC susceptible *P. radiata* and the resistant *P. pinea* after artificial inoculation with *F. circinatum*. This approach contributes to obtain valuable knowledge regarding forest trees defense response against biotic stress, and to support the development of innovative and eco-friendly disease control measures based on an early detection of PPC.

2. Material and Methods

2.1 Fungal culture and plant material

The *Fusarium circinatum* isolate FcCa6 was grown in potato dextrose agar (PDA; VWR Chemicals, Leuven, Belgium) at 25 °C until 90% of the Petri dish was covered by mycelium [20]. Three plugs of mycelium (5 mm diameter) were cut and grown under agitation on potato dextrose broth (PDB; CONDA, Madrid, Spain) for 24 h and the spores were counted (using a haemocytometer). Spores solution was adjusted to 10⁴ spores mL⁻¹ before plant inoculation.

Six-month-old *P. radiata* and *P. pinea* seedlings were obtained from Melo & Cancela Lda. (Anadia, Portugal). The plants were transplanted to 400 mL pots containing a 3:2 (w/w) peat:perlite mixture and kept in a greenhouse under semi-controlled day/night conditions (25/20 °C temperature, 60/65% relative humidity and natural photoperiod and photosynthetic active radiation). Plants were acclimatized for 1 month, being watered every two days and fertilized weekly with N:P:K solution ((5:8:10), (Nutrea, Genyen, Mafra, Portugal)

2.2 Plant inoculation and experimental design

After acclimatization, seedlings of each pine species were separated into two groups of 12 seedlings each: controls (C) vs. inoculated with *F. circinatum* (F). Ten µL of spore's suspension (corresponding to a final concentration of 10⁴ spores mL⁻¹) were applied after stem wounding using a sterile scalpel and the wound was then sealed with Parafilm®. Controls were mock-inoculated with 10 µL of PDB. Plants were kept under the environmental conditions previously described. Several sampling points were considered after inoculation with *F. circinatum*: 0 (F0), 3 (F3), 6 (F6), 8 (F8), 10 (F10), 14 (F14), 17 (F17), and 21 (F21) days post-inoculation (dpi). In addition to visual monitorization of disease symptoms, stem cuts were used to evaluate relative internal necrosis and for histological analysis by optical microscopy and RS analysis.

2.3 Visual symptoms and relative internal necrosis

Visual symptoms (tip dieback, needle wilting and chlorosis) were recorded daily to follow disease progression. For each time point, relative internal stem lesion length of three biological replicates *per* species and group was measured in longitudinal stem cuts, as the relation of

internal lesion length to the total stem length. The presence of *F. circinatum* in inoculated seedlings was confirmed by plating stem cuts in PDA at 25°C, followed by identification of the pathogen through micromorphological analysis. Relative internal necrosis data were determined through generalized linear models (GLM). Data was checked for normality and homoscedasticity using Shapiro–Wilk and Levene’s tests, respectively. A one-way ANOVA followed by Tukey’s HSD test with Benjamini-Hochberg correction was performed to identify differences between means across treatments. Different letters indicate significant differences ($p < 0.05$) between time points on inoculated plants. Statistical analysis were performed using the R software environment version 3.4.2 (R Foundation for Statistical Computing, <http://www.R-project.org>) employing the “fitdistrplus” package ^[37].

2.4 Histological sectioning

Histological sections were obtained according to the method of Lopes ^[38]. Briefly, the stem cuts (at the inoculation point) were conserved in 70% ethanol and paraffin-embedded, and 50 µm transversal sections were cut using a sliding microtome (Jung AG Heidelberg, Germany). These sections were clarified in a solution of sodium hypochlorite, neutralized for 5 min in 1% acetic water (*v/v*) and washed with distilled water. These were then double-stained with iodine green (10 sec) and alum carmine (10 min) and dehydrated using a series of ethanol-based solutions: 70% ethanol (3 min), 90% ethanol (3 min), absolute ethanol and absolute ethanol:xylol (1:1 *v/v*, for 5 min).

Samples were mounted in glass microscope slides using Entellan. Definitive preparations were observed under an optical microscope (DS-U3, Nikon Instruments Europe B.V., Netherlands) coupled to a high-resolution digital microscope camera (DS-Ri1, Nikon Instruments Europe B.V., Netherlands). Histological sections were obtained in three biological replicates from each species and group.

2.5 Raman Microspectroscopy

2.5.1 Sample preparation

At each time point, the main stem from both species and groups (one biological replicate from inoculated and one from control groups) were longitudinally cut 0.5 cm above the inoculation point (approximately 1 cm long). The stem cuts were immediately measured by Raman microspectroscopy, along the xylem and phloem regions. The Raman spectra were recorded in the 450–3750 cm^{-1} range using a WITec confocal Raman microscope system alpha300R coupled to an Ultra-High-Throughput-Spectrometer UHTS 300 Vis-NIR (300 mm focal length, 600 grooves/mm blazed for 500 nm grating). The detection system consisted of a thermoelectrically cooled CCD (charge-coupled device) camera with a Peltier cooling system (reaching a temperature ≤ -55 °C) and a chip with 1650×200 pixels, front-illuminated with NIR/VIS anti-reflection coating and spectral resolution < 0.8 cm^{-1} /pixel. The excitation radiation used was a 532-nm laser, yielding 20–22 mW at the sample position. An objective Zeiss "Epiplan" 10x (NA 0.23; WD 11.1 mm) was used. For each time point, a total of 200 spectra were collected *per* sample (covering 40 different regions *per* sample, and 5 spectra *per* region), enabling to encompass the tissue heterogeneity. Each individual spectrum was recorded with 5 accumulations and 10 s of exposure time.

2.5.2 Raman spectroscopy data pre-processing

The Raman background originated from the optics was subtracted from all spectra. A principal-component (PC)-based noise reduction algorithm retaining a selected number of principal components (20 PC's) was applied and the dataset was then recombined. Fixed-pattern interference in the Raman spectra generated by the detector response was removed using a 3rd-order spline function. All spectra were cropped into two spectral intervals: fingerprint region (1000-1800 cm⁻¹) and high wavenumber region (2800-3150 cm⁻¹). The spectra were scaled to the average of all individual spectra using the extended multiplicative signal correction (EMSC) with a 1st-order polynomial background [39]. For each region, the Raman spectra from 5 measurements were averaged (*per* measured region).

2.5.3 Raman spectroscopy data analysis

The analysis of the Raman spectroscopy data was designed to explore spectral constitutive and induced traits. In order to analyse the constitutive differences among the different species (*P. radiata* controls vs. *P. pinea* controls), the Raman spectra collected from all control samples at all time points were analysed by unsupervised principal component analysis (PCA). Average Raman spectra were computed from all control samples for each species, for comparison, and the spectral signals were assigned to major sample constituents (Table 1). To assess the main differences among the two species after fungal infection over time (*P. radiata* inoculated vs. *P. pinea* inoculated), the Raman spectra from inoculated samples from both species were analysed by PCA, for each time point.

In order to investigate potential induced spectral changes that may support early detection the trend of the spectral contribution from antisymmetric and symmetric $\nu(\text{COC})$ glycosidic vibrational modes was evaluated over time after fungal inoculation. The choice of these bands followed the results obtained from the PCA analysis. The spectral range including these bands was integrated (1090 -1145 cm⁻¹) and the ratio between control and inoculated spectra was computed for each species, *per* time point. For this purpose, a randomized average of control spectra from all time points was calculated in order to obtain representative Raman spectra from control samples and to minimize sample variability. A randomized average was performed so that the control group had a similar size to the inoculated one, for each time point and for each species.

All computations and multivariate analysis were carried out using Matlab 2019a (The MathWorks Inc., Natick, MA) and in-house developed routines. For the t-tests on spectral data to unveil the underlying chemometric relationships between Raman spectra an R-based data analysis platform was used [40].

3 Results

3.1 Disease symptoms and stem relative internal necrosis

The first external symptoms of PPC (needle wilting and tip dieback) were detected in inoculated *P. radiata* 9 days post-inoculation (dpi). No visible PPC symptoms were found in *P. pinea* throughout the entire experiment. Stem relative internal necrosis was significantly increased in *P. radiata* seedlings 8 dpi (1.4 %), reaching its maximum at 21 dpi (11.3 %) (Fig. 1); while stem internal necrosis was not observed in *P. pinea*.

3.2 Histological analysis

Histological sections allowed to observe the result of hosts' tissues colonization by *F. circinatum*, through anatomical changes at different sampling points. In *P. radiata* inoculated samples, visual damages and disruption of the pith was visible from 6 dpi onwards (Fig. 2). In *P. pinea* no changes were observed upon *F. circinatum* inoculation. Additionally, *F. circinatum* inoculation was not found to elicit changes in resin ducts density in either species. Constitutive anatomical differences between *P. radiata* and *P. pinea* were observed, highlighting a thicker cortex and smaller resin ducts in *P. pinea* when compared to *P. radiata* (Fig. 2).

3.3 Raman Spectroscopy

3.3.1 Constitutive Differences

Figure 3 comprises the average Raman spectra of *P. pinea* and *P. radiata* control samples in the 400-1800 cm^{-1} and 2400-3800 cm^{-1} spectral regions, with one of the most prevailing sample constituents (α -cellulose) being plotted for comparison. The raw and preprocessed Raman spectra from *P. pinea* and *P. radiata* samples are shown in Supplementary Material (Fig. S1). The tentative Raman assignments of the main spectral signals are shown in Table 1. When comparing *P. radiata* and *P. pinea* control samples, it is clear that the spectral differences are mainly associated to lignin, cellulose, heteromannans and heteroxylans. With respect to lignin, the key signals are assigned to derivatives such as coniferaldehyde and coniferyl alcohol. Concerning the cellulose, an α -cellulose standard has been measured to identify its main spectral contributions in both species. Although some structural differences are expected between native cellulose and α -cellulose such as the propensity for depolymerisation/hydrolysis in aqueous basic media, the presented data enables the identification of cellulose characteristic signals belonging to cellulose; particularly, the signals located in the range between 1000-1500 cm^{-1} being the most important those that belong to COC glycosidic (asymmetric, 1102 cm^{-1} , and symmetric stretching vibrations, 1133 cm^{-1}) mainly from cellulose, heteromannans and heteroxylans; CH_2 (scissoring deformation at 1470 cm^{-1} for α -cellulose shifted to *ca.* 1460 cm^{-1} in both species, and deformation at 1383 cm^{-1} for α -cellulose shifted to *ca.* 1371 cm^{-1} in both species).

To characterize the main spectral differences between the *P. radiata* and *P. pinea* the Raman spectra collected from all control samples at all time points were analysed by unsupervised principal component analysis (PCA). Figure 4a represents the score plot for the two first principal components, PC-1 vs PC-2, comprising 43.3% and 27.6% of the total variance, respectively. A clear separation between *P. pinea* and *P. radiata* controls is observed along PC-1. Figure 4b shows the loading plot of PC-1 in the fingerprint spectral range, 1000-1800 cm^{-1} . It is noteworthy that the separation between species is mainly due to a shift of the signal at *ca.* 1600 cm^{-1} (Fig. 4b), which is ascribed to the aromatic ring symmetric stretch from lignin. This feature is consistent at all time points.

3.3.2 Spectral differences highlighted with *F. circinatum* inoculation

The Raman spectral differences between *P. pinea* and *P. radiata* after inoculation with *F. circinatum* were evaluated by PCA. Figure 5 shows the PCA score plots and loadings extracted for the principal components PC1 vs PC2 from *P. radiata* vs *P. pinea* inoculated samples (in

the fingerprint spectral range, 1000-1800 cm^{-1}) over 21 dpi. From the score plots in Figure 5 (left side) it is evident that the two species are separated along the first principal component (PC-1) at all time points. The loading plots (on the right-hand side) give an insight of the chemical components responsible for such separation. It is important to note that, at 1 dpi the separation between species is mainly due to the shift of the signal at *ca.* 1600 cm^{-1} ascribed to the aromatic ring symmetric stretch from lignin, as also observed in the control groups (see Fig. 4). On the other hand, from 3 dpi onwards, the separation starts to have contributions from the (COC) glycosidic antisymmetric and symmetric stretching bands (1090-1145 cm^{-1}) assigned to cellulose, heteromannans and heteroxylans, which are polysaccharides present in the plant cell wall. It is noteworthy that the differences attributed to the response to *F. circinatum* from each of the pine species are due to these bands, consistently at all time points after day 3 up to 21 dpi (Fig. 5).

Figure 6 depicts the trend of the control/inoculated ratio computed based on the integration of antisymmetric and symmetric $\nu(\text{COC})$ glycosidic bands (1090-1145 cm^{-1}) over the 21 days after inoculation. This plot highlights the significant differences found between *P. radiata* and *P. pinea* samples within this spectral region from 3 dpi onwards, which are likely linked to structural rearrangements after fungal inoculation in the susceptible *P. radiata*.

For the spectral differences between *P. radiata* inoculated and non-inoculated with *F. circinatum*, a supervised approach consisting of t-tests ($p \leq 0.0001$) followed by PCA of the most significantly different wavenumbers was employed. This allowed to understand the chemometric differences between *P. radiata* inoculated and non-inoculated control samples. Differences were primarily visible at 3, 6, 8, 10 and 14 dpi (Fig. 7), with gradually fewer differences between the two groups as time post-inoculation progresses. Most bands that are highlighted in inoculated samples were ascribed to phenolic components, namely to lignin (Table 2). Conversely, in control samples most bands were ascribed to cellulose, heteromannans and heteroxylans. At 1, 17 and 21 dpi, no separation was found between *P. radiata* inoculated and control samples.

4. Discussion

4.1.1 Constitutive differences between *Pinus* spp. — lignin composition as a key PPC defence trait

Although this study was mainly aimed at evaluating changes occurring after pathogen infection, *P. radiata* and *P. pinea* also revealed to be constitutively different. From the analysis of the corresponding histological sections, it was observed that *P. pinea* stems possess a thicker cortex than that of the susceptible *P. radiata*. This may contribute to *P. pinea* resistance to *F. circinatum* infection by rendering the access of *F. circinatum* more difficult to the host phloem, xylem and pitch for further colonization. Furthermore, xylem resin ducts from *P. radiata* appear to be larger in comparison to *P. pinea*. Resin ducts have been widely associated as a key player in conifers' defense mechanisms against pathogens^[41]. However, in our pathosystem this may not constitute an advantage as Martín-Rodríguez *et al.* (2013) observed that upon inoculation, resin ducts were vertically colonized by *F. circinatum* in *P. radiata* seedlings^[6]. Also, a denser resin duct network with smaller ducts may confer greater resistance to pathogens than a low-density network of large resin ducts^[41]. For example, *Pinus strobus* L. presents fewer but larger inner resin ducts than some spruce species, which favored weevil (*Pissodes strobe*) body mass gain^[42]. This structure

may make it easier for biotic agents to access their hosts as there are more resin-free areas. Despite this may in part explain the difference in susceptibility between *P. radiata* and *P. pinea*, further studies are needed to validate this hypothesis. Regarding RS results, the main differences were reflected in a shift of the band assigned to the aromatic ring symmetric stretch from lignin (1602-1604 cm^{-1}) to higher wavenumbers (1607 cm^{-1}) in *P. radiata* control samples. This suggests that the distribution of the lignin subunits is heterogeneous, depending on the sample and the complexity of the polymer [43]. Actually, lignin and lignification processes play a pivotal role in plant-pathogen interaction as a first line defence against pathogens in woody plants [56, 57]. Lignin is biosynthesized through the phenylpropanoid pathway, which is responsible for the production of key defence-related metabolites such as phenolic compounds and phenol-polyamine derivatives [58, 59], and is required for conifers defence against invasive pathogens [60, 61]. The relevance of this metabolic pathway for the *Pinus-F. circinatum* pathosystem has been recently reviewed [50] and significantly higher levels of constitutive total phenolics have been found in *P. pinea* needles when compared to *P. radiata* [22]. Moreover, previous RS studies also suggested the existence of a constitutive protection against *Ophiostoma novo-ulmi* in a less susceptible hybrid (*Ulmus minor* x *Ulmus pumila*) based on the detection of higher values of lignin in control samples in comparison with the susceptible *Ulmus minor* [28].

The key signals associated to lignin are ascribed to subunits such as conyferaldehyde and conyferyl alcohol. It is remarkable that, despite the low amounts of some constituents of the lignin polymer such as coniferyl alcohol (2%) and aldehyde (4%), these could still be detected through high intensity Raman bands due to the expected signal enhancement induced by charge transfer processes and extended electron clouds, with the consequent pre-resonant effect [51]. Some authors have described several problems regarding the decomposition of lignin subunits under laser radiation, with consequent spectral modifications mainly within the 1660/1600 cm^{-1} range, regarding the band intensity ratio of the coniferyl alcohol [52]. This effect was found to be proportional to the laser power (having been detected for 10-30 mW of a 532-nm excitation wavelength). Nevertheless, these authors also concluded that this interference occurs only in the first few seconds of laser incidence (0.05 - 5s), while for longer radiation exposures (above 5 s and up to 20 s) the ratio remains constant. Thus, it is expected that with the experimental conditions presently used this issue does not impose a problem. Since the Raman signal was collected with long exposure times (5 spectra per region, 50 seconds for each spectrum), with the laser focus remaining on the same spot for more than 4 minutes, it is safe to assume that the Raman intensity of the coniferyl alcohol signal did not undergo further changes. Moreover, all samples were subjected to the same experimental conditions, and consequently these are not expected to have any impact in the observed differences (beyond the scale error itself).

4.1.2 Interaction between *Pinus spp.* and *F. circinatum* – cell-wall degradation and synthesis of phenolic compounds in the susceptible *P. radiata*

Upon inoculation with *F. circinatum*, *P. radiata* and *P. pinea* samples showed different responses to PPC. *Pinus radiata* displayed the first external disease symptoms 9 dpi (needle wilting and tip dieback), significantly higher stem relative internal necrosis 8 dpi, and damages in the pith 6 dpi. In turn, no changes were found in *P. pinea* during the whole experiment time

course (21 days). These results are in accordance with previous PPC studies comparing *P. radiata* and *P. pinea* responses to *F. circinatum* infection^[10, 34], where *P. radiata* showed PPC symptoms between 7 and 10 dpi while, for the same period, *P. pinea* didn't show any symptoms^[10], as well as with confocal optical microscopy analysis in *P. radiata* where pith collapse was also observed^[6].

Through analysis of the Raman spectra (PC-1 loadings in Fig. 5), it is noticeable that the loadings from 1 dpi does not differ from the ones obtained in the PCA between species in control samples, as the same contributions are present (Fig. 4b). However, from 3 dpi onwards it is perceptible that another spectral contribution has arisen as responsible for the separation between the inoculated samples of the pine species studied: the antisymmetric and symmetric $\nu(\text{COC})$ glycosidic modes (at 1102 cm^{-1} and at 1133 cm^{-1} , respectively) assigned to cellulose, heteromannans and heteroxylans. Even though the main constitutive spectral contributions (spectral shift of the aromatic ring symmetric stretch from lignin) remain over the 21 dpi, the variance analysis captured on the PC1 loading over this timeline demonstrates the increasing importance of the $\nu(\text{COC})$ glycosidic vibration for the species differentiation regarding their response to *F. circinatum*. The higher control/inoculated ratio observed in *P. radiata* from 3 dpi onwards (Fig. 6, $p < 0.01$) indicates that after inoculation with *F. circinatum* this pine species undergoes structural changes that prompt an intensity decrease of the antisymmetric and symmetric $\nu(\text{COC})$ glycosidic Raman signals, whereas this effect is not perceptible in *P. pinea*. Variations in the intensity of the $\nu(\text{COC})$ glycosidic bands at *ca.* 1102 and 1126 cm^{-1} are expected to be detected as cellulose degradation occurs, because of the rupture of the bond responsible for the polymer^[53]. Therefore, these results suggest that this degradation starts soon after *F. circinatum* inoculation in *P. radiata* but not in *P. pinea*, reflecting the high level of resistance to this pathogen for the latter.

In fact, it is known that *F. circinatum* initially colonizes the host by occupying intercellular spaces, segregating extracellular enzymes that degrade the host cell wall and release large amounts of nutrients from the cells^[6]. This could be the case of: laccases, which enhance *F. circinatum* pathogenicity by rendering cellulose accessible to other enzymes and acting as an initial infection tool to overcome tree defences^[64, 65]; or endopolygalacturonase, which has its gene well-characterized in *F. circinatum* and is involved in the digestion of polysaccharides present in primary cell walls^[56]. Even though it would be ideal to detect the presence of these enzymes through RS, their contribution to the total analysed biomass is negligible.

Raman spectroscopy of *P. radiata* samples also indicated that the differences between inoculated and control plants were more notorious at 3, 6, 8, 10 and 14 dpi (Fig. 7). The interpretation of the Raman data pointed out that the synthesis of phenolic compounds seems to be upregulated in inoculated plants (Table 2). In addition to the importance of constitutive phenolics in tree resistance to pathogens (previously discussed), phenolic compounds are known to play an active role in plant defence upon fungal invasion. For example, rapid lignin deposition in the secondary cell wall is known to be involved in plant defence against pathogens^[57]. The induction of the phenylpropanoids pathway has been previously reported in *P. radiata* after *F. circinatum* infection^[16, 35, 72], with recent proteomics studies suggesting that the host's secondary metabolism (*e.g.* lignans biosynthesis) may be targeted by the pathogen to negatively regulate pine immune response^[13]. This is in accordance with the higher levels of phenolic compounds detected in inoculated *P. radiata* by RS. Raman data further indicates

differences in the lignin subunits deposited in inoculated *P. radiata* plants, and thus structural differences in the lignin between inoculated and non-inoculated samples. This could explain the higher signals observed for certain phenolic compounds in inoculated samples. As for the remaining sampling times, it is likely that differences were not detected due to (1) the fungal infection not reaching levels that would cause a metabolic response in the plant (1 dpi) or (2) the impact of advanced stem internal necrosis in RS measurements (17 and 21 dpi).

Conclusions

Besides shedding light on constitutive components that may be crucial to determine PPC resistance (such as lignin), this study reveals the potential of Raman spectroscopy as a promising tool for: (1) the early detection of PPC; and (2) the discrimination of PPC susceptibility between different species of pine trees. However, a wider screening should be performed with trees of known susceptibility to PPC in order to establish spectral signatures that may be accurately related to resistant phenotypes and to their lignin composition, aiming to fully validate this method for tree selection. Regarding the RS detection potential, while in inoculated *P. radiata* histological and relative stem internal necrosis changes were only visible at 6 and 8 dpi, respectively, Raman spectral variations could already be detected at 3 dpi, reducing by half the disease detection time in this species. The main difference observed in the response to *F. circinatum* between the pine species studied were associated to the early degradation of cellulose and upregulation of phenolic compounds synthesis in the susceptible *P. radiata*. Earlier detection of the disease would enable a faster and efficient response from a plant management perspective. This may include (i) eradication measures such as the destruction of the infected plant material and intensive surveillance, (ii) communication with nurseries and its customers to avoid the spread of the pathogen, and (iii) tracing-back studies to identify the possible source of infection. The early detection of *F. circinatum* in France and Italy was crucial to eradicate it by rapidly applying surveillance and control measures ^[74].

Besides further Raman studies are needed in order to validate this technique as a reliable technology for routine disease detection and tree selection, our results suggest the potential of RS-based approaches to find adequate eco-friendly responses to new and/or emerging plant pests and for PPC control and management. Even though this study focuses on a destructive sample approach, one can possibly foresee RS applications for early PPC detection in a minimally invasive way, e.g. by sampling needles or external parts of stem. It is however important to refer that this approach as it is would not be able to detect the presence of *F. circinatum* in resistant trees, where it could still represent a source of inoculum for nearby susceptible individuals.

Conflicts of interest

There are no conflicts to declare.

Acknowledgements

This research was performed under the framework of the PineWALL project (PTDC/ASP-SIL/3142/2020), supported by the Portuguese Foundation for Science and Technology (FCT); the URGENTpine project (PTDS/AGR-FOR/2768/2014) which is supported by FEDER

through COMPETE (Programa Operacional Fatores de Competitividade) (POCI-01-FEDER-016785) and by the Portuguese Foundation for Science and Technology (FCT); and of the F4F – Forest For Future project (CENTRO-08-5864- FSE-000031) through Programa Operacional Regional do Centro (Centro 2020) from Portugal 2020 and Fundo Social Europeu.

Thanks are due to FCT/MCTES (Ministry for Science, Technology and Higher Education) for financial support to QFM-UC (UIDB/00070/2020, UIDP/00070/2020) and CESAM (UID/50017/2020, UIDB/50017/2020, LA/P/0094/2020) through national funds. FCT also supported JA (SFRH/BD/120967/2016) and PM (SFRH/BD/143879/2019).

References

- [1] FAO, Global Forest Resources Assessment 2020: Main report, Food and Agriculture Organization of the United Nations, **2020**.
- [2] FOREST EUROPE 2020: State of Europe's Forest 2020, (Ed. R. Raši), Ministerial Conference on the Protection of Forests in Europe, **2020**.
- [3] M. J. Wingfield, A. Hammerbacher, R. J. Ganley, E. T. Steenkamp, T. R. Gordon, B. D. Wingfield, T. A. Coutinho, *Australas. Plant Pathol.* **2008**; *37*, 319.
- [4] R. N. Sturrock, S. J. Frankel, A. V. Brown, P. E. Hennon, J. T. Kliejunas, K. J. Lewis, J. J. Worrall, A. J. Woods, *Plant Pathol.* **2011**; *60*, 133.
- [5] A. Santini, L. Ghelardini, C. Pace, M. L. Desprez-Loustau, P. Capretti, A. Chandelier, T. Cech, D. Chira, S. Diamandis, T. Gaitniekis, J. Hantula, O. Holdenrieder, L. Jankovsky, T. Jung, D. Jurc, T. Kirisits, A. Kunca, V. Lygis, M. Malecka, B. Marcais, S. Schmitz, J. Schumacher, H. Solheim, A. Solla, I. Szabò, P. Tsopelas, A. Vannini, A. M. Vettraino, J. Webber, S. Woodward, J. Stenlid, *New Phytol.* **2013**; *197*, 238.
- [6] N. Martín-Rodrigues, S. Espinel, J. Sanchez-Zabala, A. Ortíz, C. González-Murua, M. K. Duñabeitia, *New Phytol.* **2013**; *198*, 1215.
- [7] T. R. Gordon, *Phytopathology.* **2006**; *96*, 657.
- [8] A. Vettraino, R. Potting, R. Raposo, *Forests.* **2018**; *9*, 568.
- [9] *EPPO Bull.* **2019**; *49*, 228.
- [10] E. U. European Commission, *Communication From The Commission to the European Parliament, the Council, the European Economic and Social Committee and the Committee of the Regions*, **2021**.
- [11] R. Drenkhan, B. Ganley, J. Martín-García, P. Vahalík, K. Adamson, K. Adamčíková, R. Ahumada, L. Blank, H. Bragança, P. Capretti, M. Cleary, C. Cornejo, K. Davydenko, J. J. Diez, H. T. D. Lehtijärvi, M. Dvořák, R. Enderle, G. Fourie, M. Georgieva, L. Ghelardini, J. Hantula, R. Ioos, E. Iturritxa, L. Kanetis, N. N. Karpun, A. Koltay, E. Landeras, S. Markovskaja, N. Mesanza, I. Milenković, D. L. Musolin, K. Nikolaou, J. A. Nowakowska, N. Ogris, F. Oskay, T. Oszako, I. Papazova-Anakieva, M. Paraschiv, M. Pasquali, F. Pecori, T. Rafoss, K. Raitelaitytè, R. Raposo, C. Robin, C. A. Rodas, A. Santini, A. V. Sanz-Ros, A. V. Selikhovkin, A. Solla, M. Soukainen, N. Soulioti, E. T. Steenkamp, P. Tsopelas, A. Vemić, A. M. Vettraino, M. J. Wingfield, S. Woodward, C. Zamora-Ballesteros, M. S. Mullett, *Forests.* **2020**; *11*, 724.
- [12] J. Amaral, B. Correia, M. Escandón, C. Jesus, J. Serôdio, L. Valledor, R. D. Hancock, L.-T. Dinis, A. Gomez-Cadenas, A. Alves, G. Pinto, *Tree Physiol.* **2021**; *41*, 801.
- [13] J. Amaral, L. Lamelas, L. Valledor, M. Á. Castillejo, A. Alves, G. Pinto, *Physiol. Plant.* **2021**; *173*, 2142.
- [14] J. Martín-García, R. Zas, A. Solla, S. Woodward, J. Hantula, E. J. Vainio, M. Mullett, C. Morales-Rodríguez, A. Vannini, P. Martínez-Álvarez, G. Pinto, A. Alves, J. Amaral, M. J. Wingfield, G. Fourie, E. T. Steenkamp, R. Ahumada, B. Šerá, A. V.

- Sanz-Ros, R. Raposo, M. Elvira-Recuenco, E. Iturritxa, T. R. Gordon, J. J. Diez, *Plant Pathol.* **2019**; *68*, 843.
- [15] S. Naidoo, B. Slippers, J. M. Plett, D. Coles, C. N. Oates, *Front. Plant Sci.* **2019**; *10*, 273.
- [16] E. A. Visser, J. L. Wegrzyn, E. T. Steenkamp, A. A. Myburg, S. Naidoo, *Microorganisms.* **2019**; *7*, 315.
- [17] L. Hernandez-Escribano, E. A. Visser, E. Iturritxa, R. Raposo, S. Naidoo, *BMC Genomics.* **2020**; *21*, 28.
- [18] A. Carrasco, J. L. Wegrzyn, R. Durán, M. Fernández, A. Donoso, V. Rodriguez, D. Neale, S. Valenzuela, *Tree Genet. Genomes.* **2017**; *13*, 46.
- [19] C. Zamora-Ballesteros, J. Martín-García, A. Suárez-Vega, J. J. Diez, *BMC Genomics.* **2022**; *23*, 194.
- [20] J. Amaral, B. Correia, C. António, A. M. Rodrigues, A. Gómez-Cadenas, L. Valledor, R. D. Hancock, A. Alves, G. Pinto, *Front. Plant Sci.* **2019**; *10*, 509..
- [21] C. Zamora-Ballesteros, G. Pinto, J. Amaral, L. Valledor, A. Alves, J. J. Diez, J. Martín-García, *Int. J. Mol. Sci.* **2021**; *22*, 5231.
- [22] F. Leitão, G. Pinto, J. Amaral, P. Monteiro, I. Henriques, *Tree Physiol.* **2022**; *42*, 600.
- [23] S. Sankaran, A. Mishra, R. Ehsani, C. Davis, *Comput. Electron. Agric.* **2010**; *72*, 1–13.
- [24] A.-K. Mahlein, *Plant Dis.* **2016**; *100*, 241.
- [25] J. S. Lupoi, E. Gjersing, M. F. Davis, *Front. Bioeng. Biotechnol.* **2015**; *3*, 50.
- [26] A. O. Conrad, P. Bonello, *Front. Plant Sci.* **2015**; *6*, 1152.
- [27] J. A. Martín, A. Solla, M. A. Coimbra, L. Gil, *Phytochemistry* **2005**; *66*, 2458.
- [28] J. A. Martín, A. Solla, S. Woodward, L. Gil, *For. Pathol.* **2007**; *37*, 187.
- [29] J. A. Martín, A. Solla, M. R. Domingues, M. A. Coimbra, L. Gil, *Environ. Exp. Bot.* **2008**; *64*, 97.
- [30] C. Villari, A. Dowkiw, R. Enderle, M. Ghasemkhani, T. Kirisits, E. D. Kjær, D. Marčiulyrienė, L. V. McKinney, B. Metzler, F. Muñoz, L. R. Nielsen, A. Pliūra, L.-G. Stener, V. Suchockas, L. Rodriguez-Saona, P. Bonello, M. Cleary, *Sci. Rep.* **2018**; *8*, 17448.
- [31] A. Conrad, C. Villari, P. Sherwood, P. Bonello, *Arboric. Urban For.* **2020**; *46*, 4.
- [32] M. Mukrimin, A. Kovalchuk, R. P. Ghimire, M. Kivimäenpää, H. Sun, J. K. Holopainen, F. O. Asiegbu, *Planta.* **2019**; *250*, 1881.
- [33] C. Farber, M. Mahnke, L. Sanchez, D. Kurouski, *TrAC Trends Anal. Chem.* **2019**; *118*, 43.
- [34] S. Weng, X. Hu, J. Wang, L. Tang, P. Li, S. Zheng, L. Zheng, L. Huang, Z. Xin, *J. Agric. Food Chem.* **2021**; *69*, 2950.
- [35] L. Mandrile, S. Rotunno, L. Miozzi, A. M. Vaira, A. M. Giovannozzi, A. M. Rossi, E. Noris, *Anal. Chem.* **2019**; *91*, 9025.
- [36] M. R. Vallejo-Pérez, J. A. Sosa-Herrera, H. R. Navarro-Contreras, L. G. Álvarez-Preciado, Á. G. Rodríguez-Vázquez, J. P. Lara-Ávila, *Plants.* **2021**; *10*, 1542.
- [37] M. L. Delignette-Muller, C. Dutang, *J. Stat. Softw.* **2015**; *64*, 4.
- [38] L. Lopes, R. Pinho, P. Silveira, H. Silva, in *Temáticas e métodos avançados para o ensino e investigação em biologia*, (Ed: F. M. A. Soares), Afrontamento, Aveiro, **2016**, pp. 506–538.
- [39] H. Martens, E. Stark, *J. Pharm. Biomed. Anal.* **1991**; *9*, 625.
- [40] Z. Pang, J. Chong, G. Zhou, D. A. de Lima Morais, L. Chang, M. Barrette, C. Gauthier, P.-É. Jacques, S. Li, J. Xia, *Nucleic Acids Res.* **2021**; *49*, W1.
- [41] C. Vázquez-González, R. Zas, N. Erbilgin, S. Ferrenberg, V. Rozas, L. Sampedro, *Tree Physiol.* **2020**; *40*, 1313.
- [42] D. Boucher, R. Lavallée, Y. Mauffette, *Can. J. For. Res.* **2001**; *31*, 2035.

- [43] U. P. Agarwal, *Molecules*. **2019**; *24*, 1659.
- [44] C. P. Vance, T. K. Kirk, R. T. Sherwood, *Annu. Rev. Phytopathol.* **1980**; *18*, 259.
- [45] N. H. Bhuiyan, G. Selvaraj, Y. Wei, J. King, *Plant Signal. Behav.* **2009**; *4*, 158.
- [46] T. Higuchi, *Biosynthesis and Biodegradation of Wood Components*, Academic Press, Orlando, Florida, **1985**.
- [47] G. G. Gross, in *Biosynthesis and biodegradation of wood components*, (Ed: T. Higuchi), Elsevier, **1985**, pp. 229–271.
- [48] J. Witzell, J. A. Martín, *Can. J. For. Res.* **2008**; *38*, 2711.
- [49] A. Ganthaler, W. Stöggl, S. Mayr, I. Kranner, S. Schüler, E. Wischnitzki, E. M. Sehr, S. Fluch, C. Trujillo-Moya, *Plant Mol. Biol.* **2017**; *94*, 229.
- [50] J. Amaral, Deciphering Pinus defence response against *Fusarium circinatum*: from physiology to Omics (PhD thesis), University of Aveiro, **2021**.
- [51] P. Bock, N. Gierlinger, *J. Raman Spectrosc.* **2019**; *50*, 6.
- [52] B. Prats-Mateu, P. Bock, M. Schroffenegger, J. L. Toca-Herrera, N. Gierlinger, *Sci. Rep.* **2018**; *8*, 11804.
- [53] H. G. M. Edwards, D. W. Farwell, D. Webster, *Spectrochim. Acta Part A Mol. Biomol. Spectrosc.* **1997**; *53*, 2383.
- [54] P. Bora, G. E. S. J. Hardy, P. A. O'Brien, *Australas. Plant Pathol.* **2005**; *34*, 591.
- [55] E. J. Muñoz-Adalia, J. A. Flores-Pacheco, P. Martínez-Álvarez, J. Martín-García, M. Fernández, J. J. Diez, *Physiol. Mol. Plant Pathol.* **2016**; *94*, 8.
- [56] P. M. Chimwamurombe, B. D. Wingfield, A.-M. Botha, M. J. Wingfield, *Curr. Microbiol.* **2001**; *42*, 350.
- [57] A. Bagniewska-Zadworna, A. Barakat, P. Łakomy, D. J. Smoliński, M. Zadworny, *Plant Sci.* **2014**; *229*, 111.
- [58] A. Donoso, V. Rodriguez, A. Carrasco, R. Ahumada, E. Sanfuentes, S. Valenzuela, *Physiol. Mol. Plant Pathol.* **2015**; *92*, 42.
- [59] A.-M. Saariaho, D. S. Argyropoulos, A.-S. Jääskeläinen, T. Vuorinen, *Vib. Spectrosc.* **2005**; *37*, 111.
- [60] A.-M. Saariaho, A.-S. Jääskeläinen, M. Nuopponen, T. Vuorinen, *Appl. Spectrosc.* **2003**; *57*, 58.
- [61] K. L. Larsen, S. Barsberg, *J. Phys. Chem. B.* **2010**; *114*, 8009.
- [62] N. Gierlinger, L. Sapei, O. Paris, *Planta.* **2008**; *227*, 969.
- [63] U. P. Agarwal, J. D. McSweeney, S. A. Ralph, *J. Wood Chem. Technol.* **2011**; *31*, 324.
- [64] P. Bock, P. Nousiainen, T. Elder, M. Blaukopf, H. Amer, R. Zirbs, A. Potthast, N. Gierlinger, *J. Raman Spectrosc.* **2020**; *51*, 422.
- [65] U. P. Agarwal, S. A. Ralph, *Appl. Spectrosc.* **1997**; *51*, 1648.
- [66] E. Wiercigroch, E. Szafraniec, K. Czamara, M. Z. Pacia, K. Majzner, K. Kochan, A. Kaczor, M. Baranska, K. Malek, *Spectrochim. Acta Part A Mol. Biomol. Spectrosc.* **2017**; *185*, 317.
- [67] M. Zhang, C. Lapierre, N. L. Nouxman, M. K. Nieuwoudt, B. G. Smith, R. R. Chavan, B. H. McArdle, P. J. Harris, *Plant Physiol. Biochem.* **2017**; *118*, 187.
- [68] D. Martin, J. Marques, A. M. Amado, M. J. Barroca, A. Moreira da Silva, L. A. E. Batista de Carvalho, M. P. M. Marques, *J. Raman Spectrosc.* **2020**; *51*, 313.
- [69] Y. Zeng, J. M. Yarbrough, A. Mittal, M. P. Tucker, T. B. Vinzant, S. R. Decker, M. E. Himmel, *Biotechnol. Biofuels.* **2016**; *9*, 256.
- [70] M. M. L. Yu, H. G. Schulze, R. Jetter, M. W. Blades, R. F. B. Turner, *Appl. Spectrosc.* **2007**; *61*, 32.
- [71] H. J. Byrne, M. Baranska, G. J. Puppels, N. Stone, B. Wood, K. M. Gough, P. Lasch, P. Heraud, J. Sulé-Suso, G. D. Sockalingum, *Analyst.* **2015**; *140*, 2066.
- [72] T. Hänninen, E. Kontturi, T. Vuorinen, *Phytochemistry.* **2011**; *72*, 1889.

- [73] D. S. Himmelsbach, D. E. Akin, *J. Agric. Food Chem.* **1998**; *46*, 991.
- [74] E. J. Vainio, D. Bezos, H. Bragança, M. Cleary, G. Fourie, M. Georgieva, L. Ghelardini, S. Hannunen, R. Ioos, J. Martín-García, P. Martínez-Álvarez, M. Mullett, T. Oszako, I. Papazova-Anakieva, B. Piskur, C. Romeralo, A. V. Sanz-Ros, E. T. Steenkamp, K. Tubby, M.J. Wingfield, J. J. Diez, *Forests.* **2019**; *10*, 9.

Accepted Article

Table 1. Tentative assignment of the main Raman signals measured for *Pinus radiata* and *Pinus pinea* control samples, and for an α -cellulose standard.

Raman shift (cm^{-1})			Tentative assignment	Possible wood components	References
α -cellulose standard	<i>P. radiata</i> (control)	<i>P. pinea</i> (control)			
440	441	441	CCO ring	cellulose	434 cm^{-1} [43] [53]
---	595w	595w	skeletal deformation of aromatic rings, substituent groups, and side chains	coniferyl aldehyde	584 cm^{-1} [51]
---	645	641	ring skeletal deformation	lignin H-units	639 cm^{-1} [59-61]
---	862vw	859vw	aromatic breathing	lignin H-units	859 cm^{-1} [60][61]
---	928	928	CCH wagging	lignin G-units	936 cm^{-1} [60]
1100	1102	1102	$\nu(\text{COC})_{\text{as}}$ glycosidic	cellulose, heteromannans, heteroxylans	1096 cm^{-1} [43][62]
1126	1133	1133	$\nu(\text{COC})_{\text{sym}}$ glycosidic $\delta(\text{CH})$ $\nu(\text{CC})$	cellulose, heteromannans, heteroxylans lignin coniferaldehyde	1122 cm^{-1} [43] [62] 1131 cm^{-1} [63] 1136 cm^{-1} [63]
1153sh	1154sh	1154sh	$(\text{C-C})_{\text{assym}}$ ring breathing	cellulose	1155 cm^{-1} [43] [62]
---	1200	1200	$\text{C}_{\text{ar}}\text{-C}$ ring deformation	lignin H units	1214 cm^{-1} [61]
---	1220vw	1220 vw	$\text{C}_{\text{ar}}\text{-O}$	lignin	1223 cm^{-1} vw [63]
---	1238 w_{sh}	1238 w_{sh}	$\nu(\text{C}_{\text{ar}}\text{-O})$ /ring deformations	lignin	1241 cm^{-1} w_{sh} [61]
---	1338	1338	$\delta(\text{C-H})$ ($\text{C}=\text{C}$)	lignin	1335 cm^{-1} [64]
1383	1371	1371	$\delta(\text{CH}_2)$	cellulose, heteromannans, heteroxylans	1377 cm^{-1} [53][65]
1470	1462	1460	$\delta(\text{CH}_2)$ scissoring		1479 cm^{-1} [53], [65] 1458 cm^{-1} [53], [65]

---	1607	1604	ν_{sym} ring)	(aromatic lignin	1600 cm^{-1} [53] [63][65]
---	1665	1662	ν (C=C) ν (C=O)	conyferyl alcohol conyferaldehyd e	1662 cm^{-1} [63] 1670 cm^{-1} [63]
2899	2902	2900	ν (CH) ν (CH ₂)	and cellulose, heteromannans, heteroxylans, lignin	2887 cm^{-1} [53][65]
---	2942	2942	ν (CH) _{as} in -OCH ₃	lignin	2940 cm^{-1} [63]
---	3076	3076	ν (C-H) aromatic	lignin	3070 cm^{-1} [63]

Abbreviations: as – antisymmetric; ar – aromatic; sym – symmetric; ν – stretching; δ – bending; w – weak; vw – very weak; vvw – very very weak; sh – shoulder.

Table 2. Tentative assignment of the main Raman signals considering *Pinus radiata* comparison between inoculated and non-inoculated (control) samples.

Raman shift (cm ⁻¹)					Tentative assignment	Possible wood components	References	Observations
day 3	day 6	day 8	day 10	day 14				
1043	---	1030	---	---	ip ring deformation and O-CH ₃ stretching mode	Phenolics (lignin G-units)	1036 cm ⁻¹ [61]	Higher in inoculated samples
1092	---	1105	---	---	$\nu(\text{COC})_{\text{as}}$ glycosidic	Cellulose, heteromannans, heteroxylans	1096 cm ⁻¹ [43][62]	Higher in control samples
1120	---	1131	---	---	$\nu(\text{COC})_{\text{sym}}$ glycosidic	Cellulose, heteromannans, heteroxylans	1122 cm ⁻¹ [43][62][66]	Higher in control samples
1167	---	1192	1187	---	C _{ar} -OH in-plane bending	Phenolics (lignin H-units)	1173 cm ⁻¹ [67]	Higher in inoculated samples
---	---	1230	1215	---	ring deform., C _{ar} -O	Phenolics (lignin H-units)	1223 cm ⁻¹ [63] 1214 cm ⁻¹ [67]	Higher in inoculated samples
---	1266	1253	1250	---	C _{ar} -O stretching	Phenolics (lignin H-units)	1256 cm ⁻¹ [67]	Higher in inoculated samples
1286	---	---	---	---	ring deformation and ip COH bending	Phenolics (lignin G-units)	1288 cm ⁻¹ [61]	Higher in inoculated samples
---	---	1351	1349	---	$\delta(\text{CH}_2)$	n/a	1348 cm ⁻¹ [68]	Higher in control samples
---	---	1393	---	---	Phenolic O-H bend + CH ₃ bend	Phenolics (lignin)	1393 cm ⁻¹ [63][69]	Higher in control samples
---	---	1413	1416	---	CH ₂ bending	Cellulose, heteromannans, heteroxylans	1413 cm ⁻¹ [67]	Higher in control samples
---	---	1431	---	---	CH ₃ bend + ring stretching	Phenolics (lignin)	1430 cm ⁻¹ [63]	Higher in control samples
---	---	1485	---	1480	$\delta(\text{CH}_2)$, $\delta(\text{CH}_3)$	n/a	1482 cm ⁻¹ [70]	Higher in control samples
---	1509	---	---	---	Aromatic ring stretch, asymmetric	Phenolics (lignin)	1508 cm ⁻¹ [63][65]	Higher in inoculated samples
---	1536	---	---	---	$\nu(\text{C}=\text{C})$	n/a	1531 cm ⁻¹ [71]	Higher in control samples
---	---	1580	1570	1582	Aromatic ring mode	Phenolics (lignin, syringaldehyde)	1583 cm ⁻¹ [72]	Higher in inoculated samples

						1586 cm ⁻¹ [73]	
1609	---	---	---	---	v _{sym} (aromatic ring) _{sym}	Phenolics (lignin)	1600 cm ⁻¹ [53], [51], [63], [65] Higher in inoculated samples

Abbreviations: as – antisymmetric; ar – aromatic; sym – symmetric; v – stretching; δ – bending; ip – in-plane; n/a – not assigned.

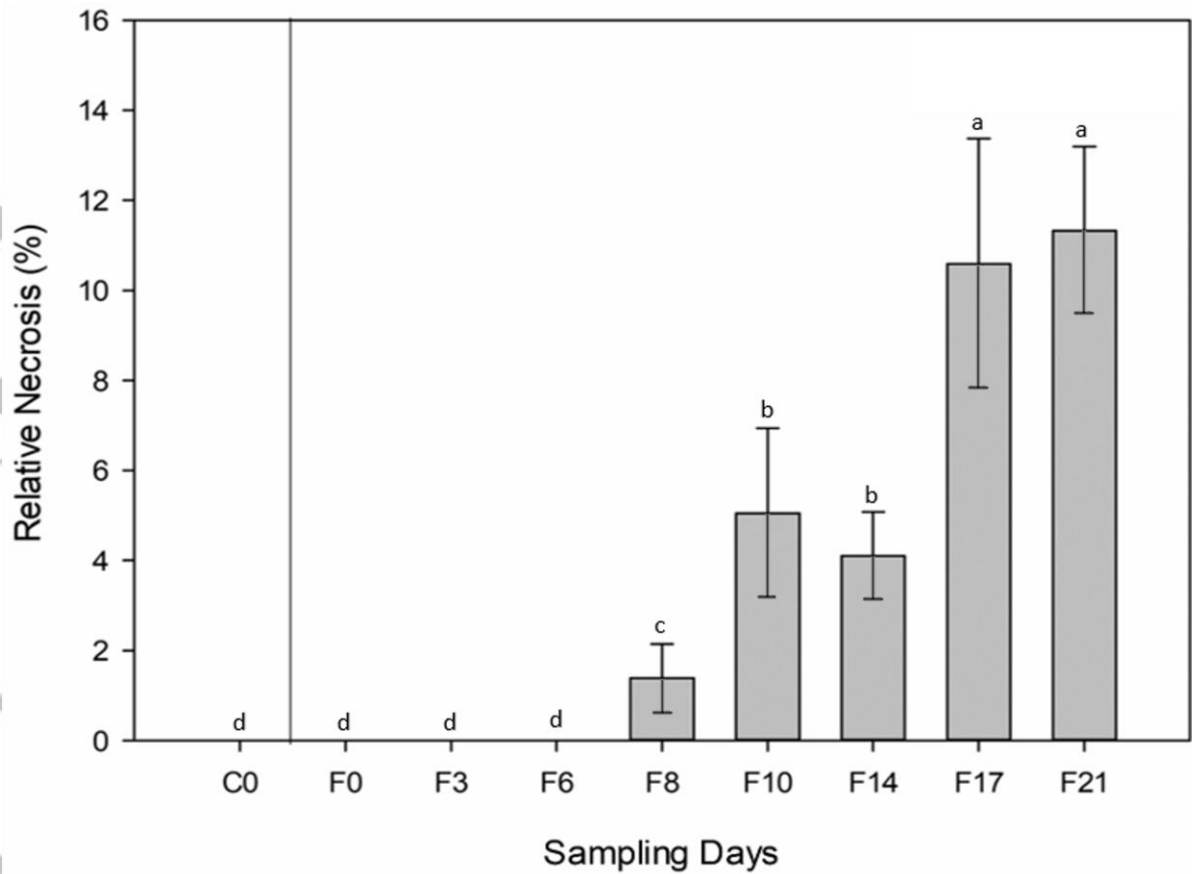


Figure 1. *Pinus radiata* stem relative internal necrosis over time. Bars show stem relative internal necrosis length (%) of inoculated plants at each time point. Relative necrosis data are presented as group mean \pm SE. Different letters indicate significantly different means at different inoculation time points (post hoc test, $p < 0.05$). No stem relative internal necrosis was found in mock-inoculated controls.

Accepted

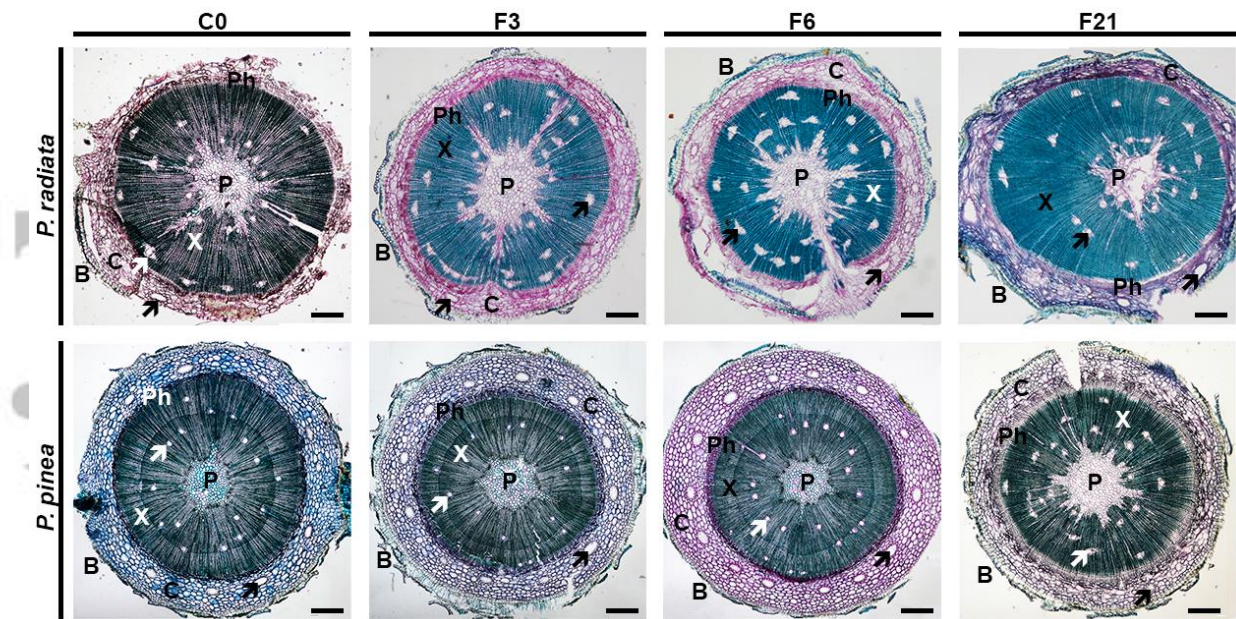


Figure 2. Histological sections from *Pinus radiata* and *Pinus pinea* stem from control (C0) and *Fusarium circinatum*-inoculated samples 3 (F3), 6 (F6) and 21 (F21) days post-inoculation. Legend: (P) pine pith; (B) pine bark; (C) pine cortex; (X) xylem; (Ph) phloem; black arrows point to resin ducts. Scale bar = 500 μ m.

Accepted

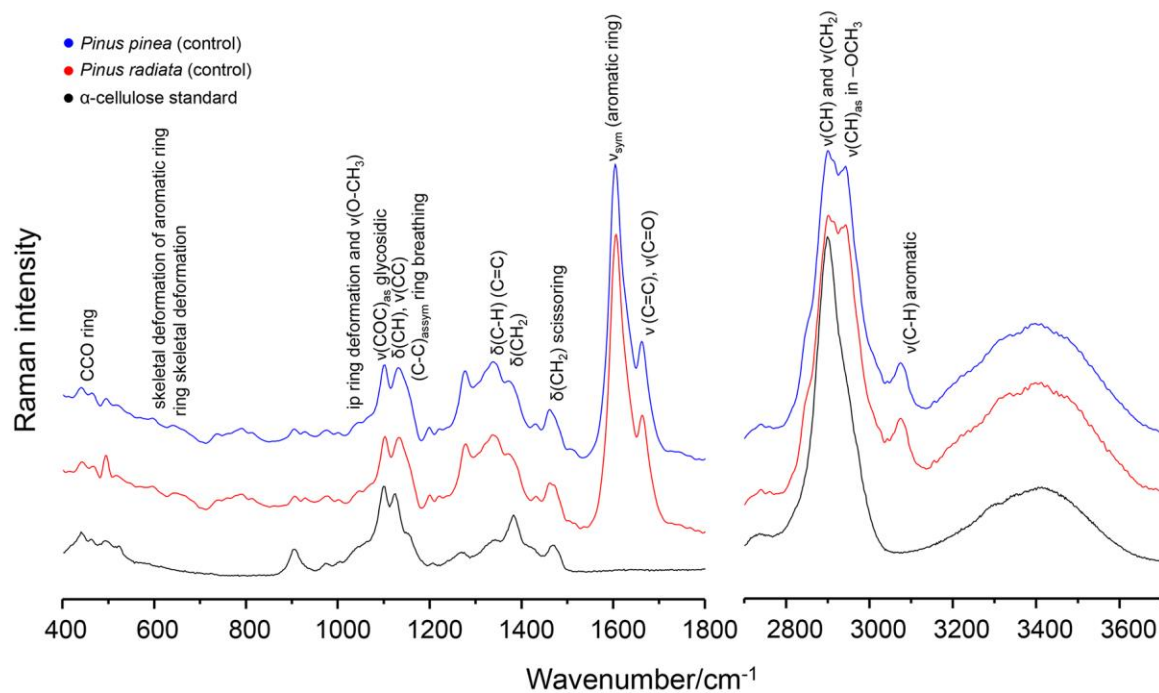


Figure 3. Average Raman spectra of *Pinus pinea* and *Pinus radiata* control samples, as well as of an α -cellulose standard. The spectra are offset along the intensity axis for clarity.

Accepted

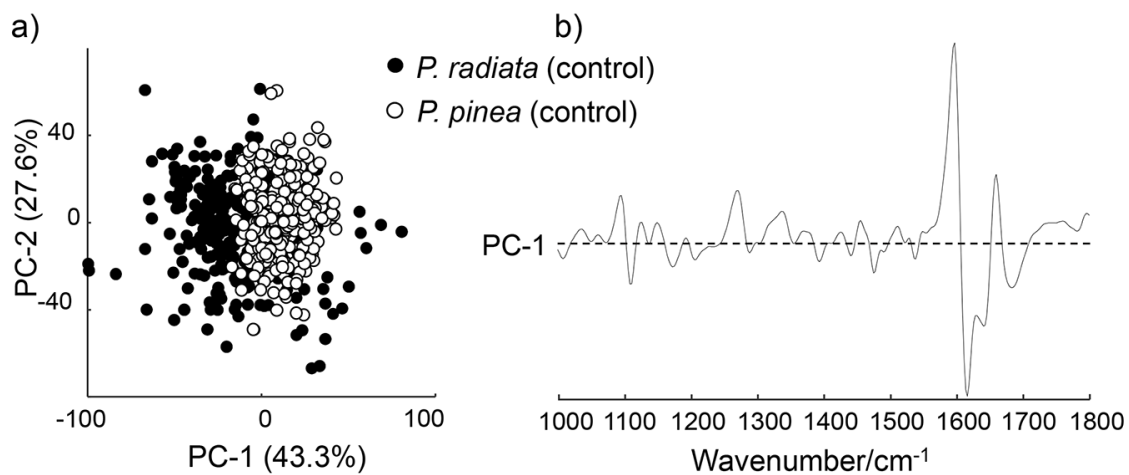


Figure 4. a) PCA scores of *Pinus radiata* vs. *Pinus pinea* control samples considering the Raman spectra in the fingerprint spectral region (1000-1800 cm⁻¹); b) PC-1 loading plot, the dashed horizontal line indicating zero loading.

Accepted Article

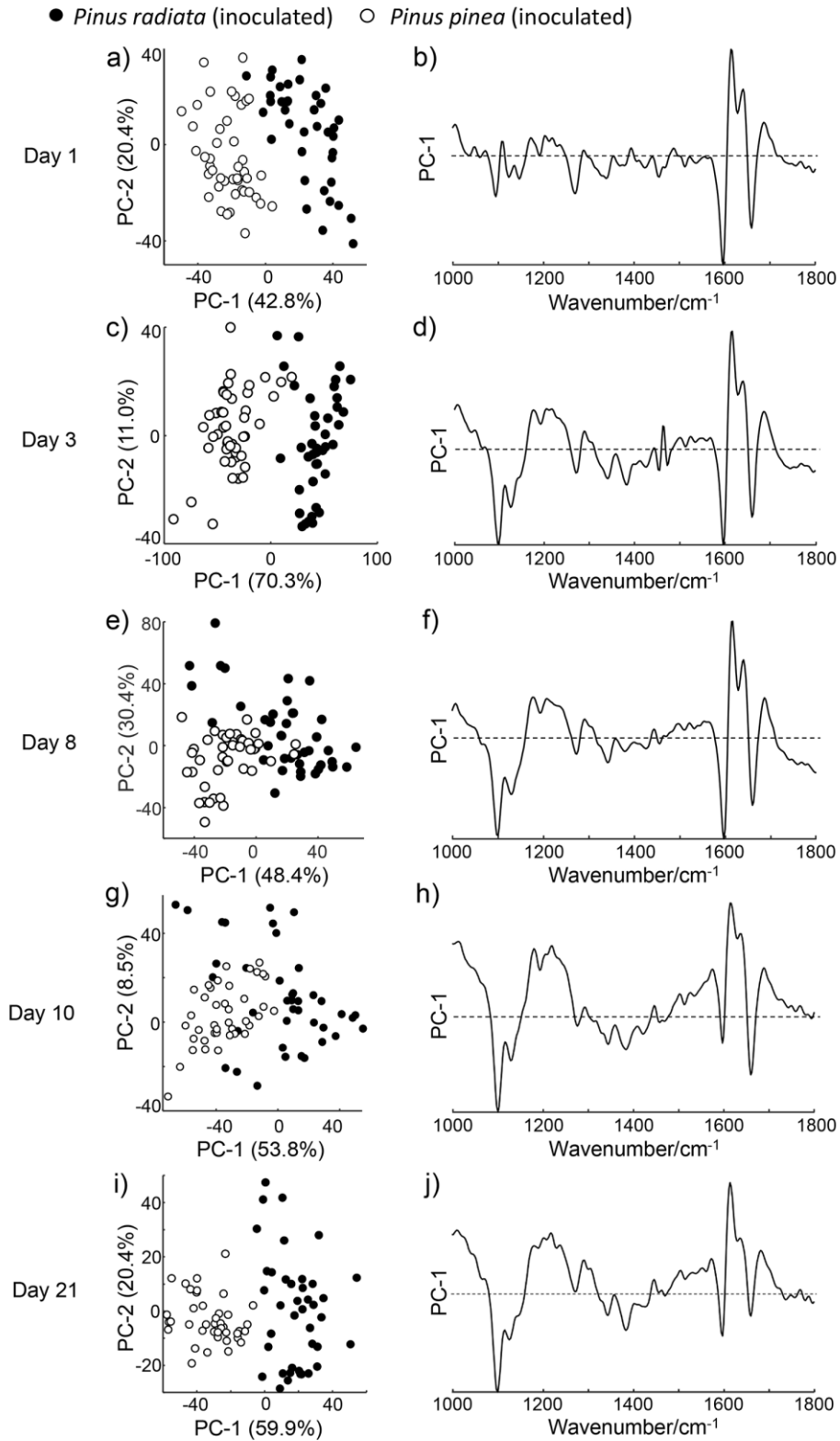


Figure 5. PC scores (left-hand side) and PC-1 loading plots (right-hand side) of *Pinus radiata* vs. *Pinus pinea* inoculated with *Fusarium circinatum*, considering the Raman spectra in the fingerprint spectral region (1000- 1800 cm⁻¹). a-b) 1 day post-inoculation; c-d) 3 days post-inoculation; e-f) 8 days post-inoculation; g-h) 10 days post-inoculation; i-j) 21 days post-inoculation. The dashed horizontal line in the PC-1 loading plots indicates zero loading.

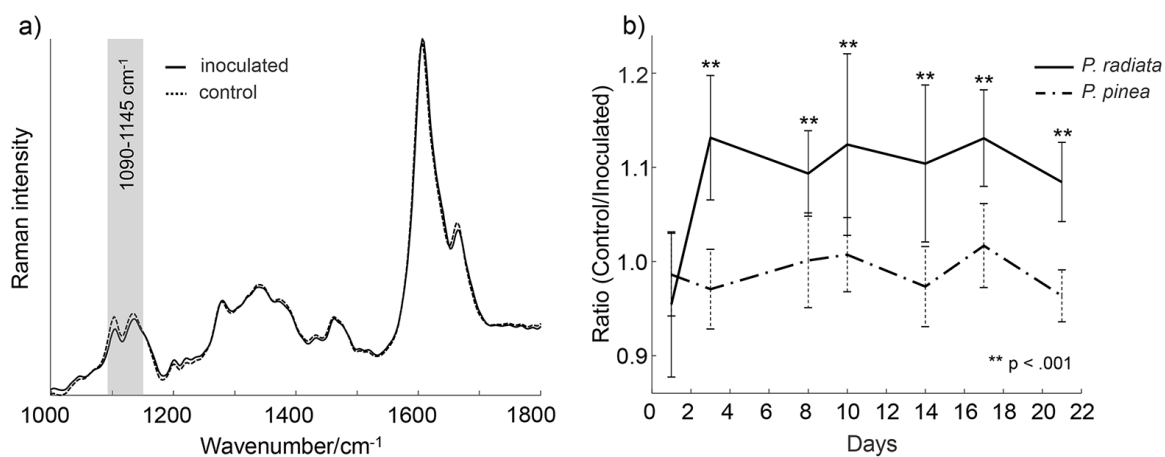


Figure 6. a) Example of an average Raman spectra of *Pinus radiata* inoculated and control samples. The integrated spectral region (1090-1145 cm⁻¹), including the antisymmetric and symmetric $\nu(\text{COC})$ glycosidic modes, was used to compute the ratio plotted in b); b) Ratio of the integrated spectral region between control and inoculated samples (for each species separately). The error bars were computed from standard deviation (using error propagation). The Student's t-test was performed to assess statistical significance.

Accepted

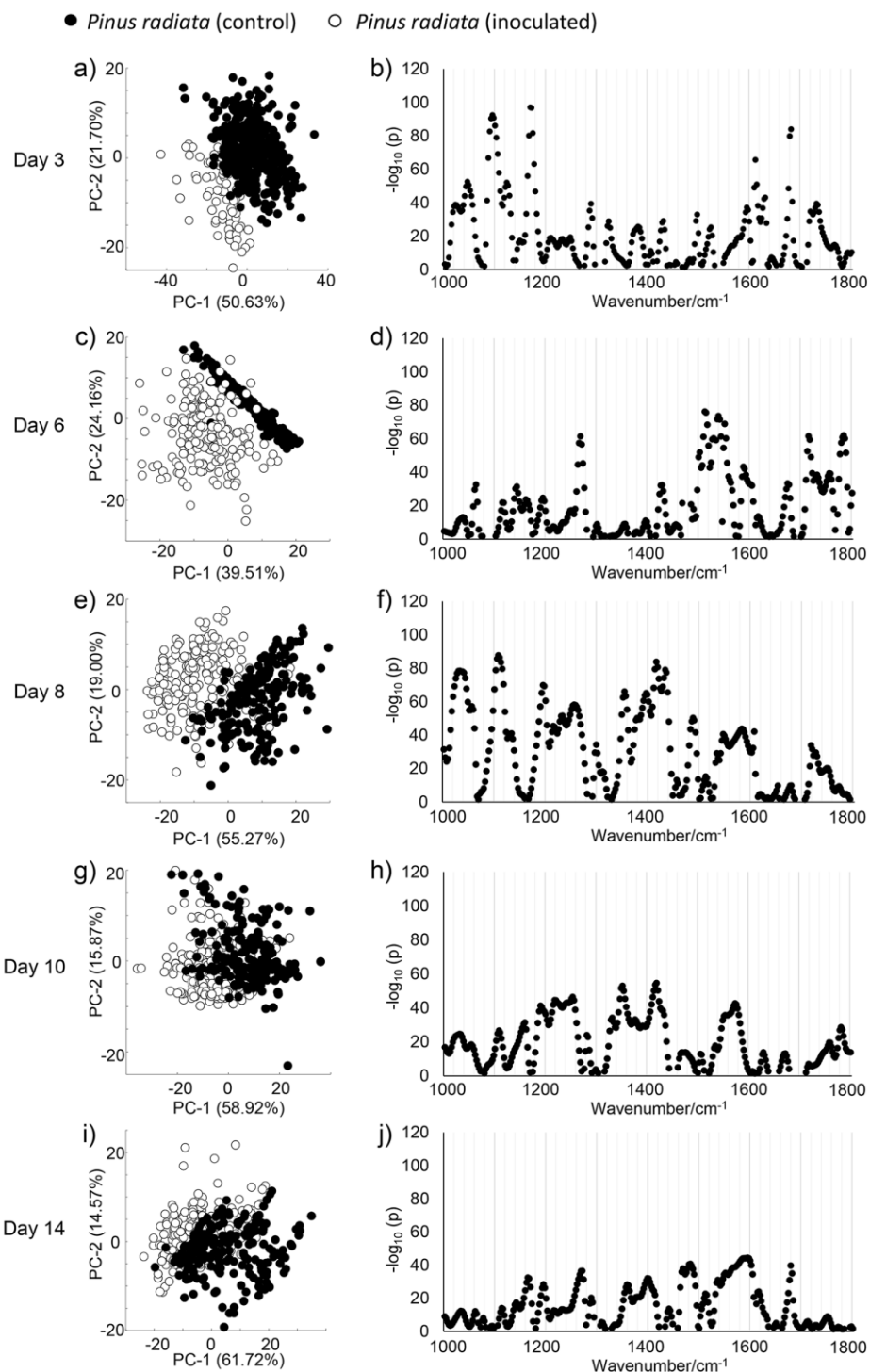
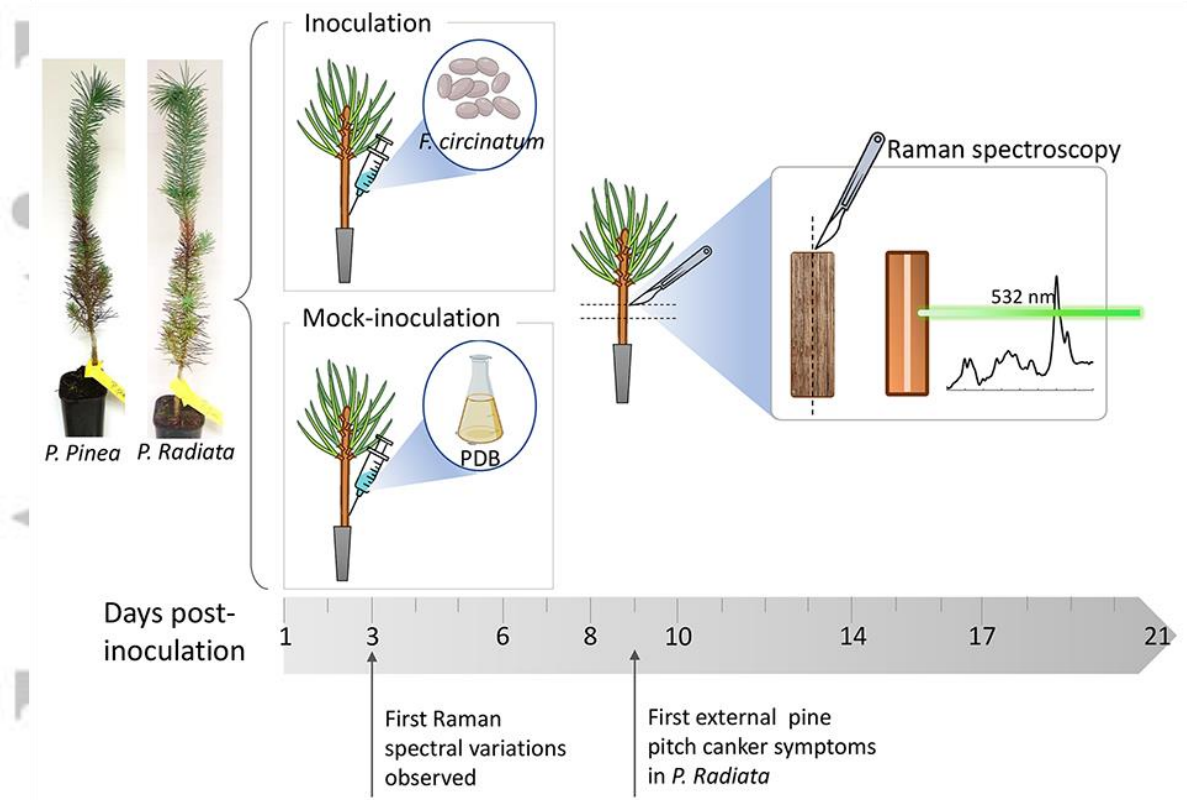


Figure 7. PC score plots (left-hand side) of *Pinus radiata* inoculated vs non-inoculated with *Fusarium circinatum*, calculated based on highly significantly different variables (t-tests, $p \leq 0.0001$, right-hand side). On the t-test plots black dots denote all the variables that are significantly different between the groups being compared ($p \leq 0.05$; $-\log_{10}(p) \geq 1.30$). a-b) 3 days post-inoculation, 249 variables; c-d) 6 days post-inoculation, 236 variables; e-f) 8 days post-inoculation, 263 variables; g-h) 10 days post-inoculation, 255 variables; i-j) 14 days post-inoculation, 223 variables.

Graphical Abstract



Accepte